

INFORMATION TO USERS

This manuscript has been reproduced from the microfilm master. UMI films the text directly from the original or copy submitted. Thus, some thesis and dissertation copies are in typewriter face, while others may be from any type of computer printer.

The quality of this reproduction is dependent upon the quality of the copy submitted. Broken or indistinct print, colored or poor quality illustrations and photographs, print bleedthrough, substandard margins, and improper alignment can adversely affect reproduction.

In the unlikely event that the author did not send UMI a complete manuscript and there are missing pages, these will be noted. Also, if unauthorized copyright material had to be removed, a note will indicate the deletion.

Oversize materials (e.g., maps, drawings, charts) are reproduced by sectioning the original, beginning at the upper left-hand corner and continuing from left to right in equal sections with small overlaps. Each original is also photographed in one exposure and is included in reduced form at the back of the book.

Photographs included in the original manuscript have been reproduced xerographically in this copy. Higher quality 6" x 9" black and white photographic prints are available for any photographs or illustrations appearing in this copy for an additional charge. Contact UMI directly to order.

UMI[®]

Bell & Howell Information and Learning
300 North Zeeb Road, Ann Arbor, MI 48106-1346 USA
800-521-0600

University of Alberta

Characterization of MDI Generated Aerosol Droplets and
Comparison to Classical Evaporation Theory

by



KIM-YEE LAI

A thesis submitted to the Faculty of Graduate Studies and Research in partial fulfilment
of the requirements for the degree of Master of Science

Department of Mechanical Engineering

Edmonton, Alberta

Spring 1999



National Library
of Canada

Acquisitions and
Bibliographic Services

395 Wellington Street
Ottawa ON K1A 0N4
Canada

Bibliothèque nationale
du Canada

Acquisitions et
services bibliographiques

395, rue Wellington
Ottawa ON K1A 0N4
Canada

Your file *Votre référence*

Our file *Notre référence*

The author has granted a non-exclusive licence allowing the National Library of Canada to reproduce, loan, distribute or sell copies of this thesis in microform, paper or electronic formats.

The author retains ownership of the copyright in this thesis. Neither the thesis nor substantial extracts from it may be printed or otherwise reproduced without the author's permission.

L'auteur a accordé une licence non exclusive permettant à la Bibliothèque nationale du Canada de reproduire, prêter, distribuer ou vendre des copies de cette thèse sous la forme de microfiche/film, de reproduction sur papier ou sur format électronique.

L'auteur conserve la propriété du droit d'auteur qui protège cette thèse. Ni la thèse ni des extraits substantiels de celle-ci ne doivent être imprimés ou autrement reproduits sans son autorisation.

0-612-40074-3

University of Alberta

Library Release Form

Name of Author: Kim-Yee Lai

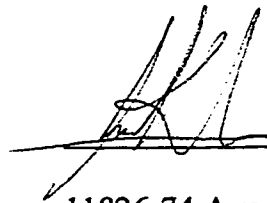
Title of Thesis: Characterization of MDI Generated Aerosol Droplets and Comparison to Classical Evaporation Theory

Degree: Master of Science

Year this Degree Granted: 1999

Permission is hereby granted to the University of Alberta Library to reproduce single copies of this thesis and to lend or sell such copies for private, scholarly, or scientific research purposes only.

The author reserves all other publication and other rights in association with the copyright in the thesis, and except as hereinbefore provided, neither the thesis nor any substantial portion thereof may be printed or otherwise reproduced in any material form whatever without the author's prior written permission



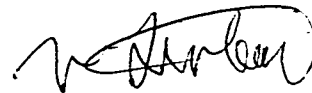
11826-74 Ave.
Edmonton AB CANADA
T6G 0G6

April. 7/99

University of Alberta

Faculty of Graduate Studies and Research

The undersigned certify that they have read, and recommend to the Faculty of Graduate Studies and Research for acceptance, a thesis entitled "Characterization of MDI Generated Aerosol Droplets and Comparison to Classical Evaporation Theory" submitted by Kim-Yee Lai in partial fulfilment of the requirements for the degree of Master of Science.



Warren H. Finlay



J. D. Dale



Peter Steffler

APR 1 1999

ABSTRACT

The validity of applying the simplified classical evaporation theory to aerosol particles emitted by metered dose inhalers (MDI) was investigated. An empty metered dose inhaler was modified to accept refills and mounted to a traverse system. The inhaler was filled with pure Freon 12 propellant to simplify the theory. Particle sizes and velocities were measured with a Dantec Phase Doppler Anemometer at various distances from the discharge nozzle. A computer program was written which predicted particle size changes based on the classical droplet evaporation theory. The theoretical results were then compared to the experimental results. The theory was found to over-predict the particle evaporation rates, yielding more particles in the $0\mu\text{m} - 10\mu\text{m}$ range and less particles in the $10\mu\text{m} - 30\mu\text{m}$ when compared to experiments. This leads to the conclusion that the classical droplet evaporation theory is unsuitable for use in predicting the particle size changes of an aerosol generated by MDI's.

ACKNOWLEDGEMENT

First of all, I would like to thank Dr. Finlay, for his technical advice, his ever-present help, his financial support, and possibly most of all his patience.

Also, thanks to the invaluable Mec. E. machine shop staff, especially Al, Tony, Albert, Max, Ian, and Bernie, for their time and for letting me pick their brains.

Thanks to my parents, for their support, both the financial and the less tangible kind. Thanks for being willing to sacrifice watching your son grow up, for the sake of his education.

And last but most of all, I want to thank Ivy. Thanks for being there for me, and for being such an awesome soul mate.

TABLE OF CONTENTS

1. INTRODUCTION.....	1
1.1 Background Information.....	1
1.2 Research Objectives.....	5
2. EXPERIMENTAL METHODOLOGY.....	6
2.1 Experimental Apparatus.....	6
2.1.1 Stage.....	6
2.1.2 Modified MDI.....	9
2.2 Measurement of Particle Velocity and Size Distributions.....	12
2.2.1 Theory of Operation of the PDA.....	12
2.2.2 Configuration of the PDA.....	14
2.2.3 Measurement Procedure.....	16
3. THEORY OF DROPLET EVAPORATION.....	18
3.1 Assumptions Required.....	18
3.2 Classical Theory.....	22
4. RESULTS AND ANALYSIS.....	31
4.1 Computer Code.....	31
4.2 Results and Analysis.....	33
4.3 Discussion of Results.....	42

5. CONCLUSIONS.....45

5.1 The Metered Dose Inhaler.....45

5.2 The Classical Droplet Evaporation Theory.....45

5.3 Future Work.....46

REFERENCES.....47

APPENDIX :Computer Code Used to Implement Classical Evaporation

Model.....48

LIST OF FIGURES

Figure 2.1: Primary Stage.....	7
Figure 2.2: Secondary Stage.....	8
Figure 2.3: Modified MDI Canister.....	11
Figure 2.4: Dantec PDA Schematic.....	15
Figure 4.1: Particle Mass Distribution at 0.004 m.....	35
Figure 4.2: Cumulative Particle Mass Distribution at 0.004 m.....	36
Figure 4.3: Particle Mass Distribution at 0.024 m.. ..	37
Figure 4.4: Cumulative Particle Mass Distribution at 0.024 m.....	38
Figure 4.5: Particle Mass Distribution at 0.044 m.. ..	39
Figure 4.6: Cumulative Particle Mass Distribution at 0.044 m.. ..	40
Figure 4.7: Droplet lifetimes as predicted by Classical Theory.....	41

NOMENCLATURE

Bi	Biot number
c	density of the vapor
c_p	heat capacity of the droplet liquid
c_s	concentration of vapor at the surface of the droplet
c_∞	concentration of vapor at infinity
D	diffusion coefficient
d	droplet diameter
d_0	initial droplet diameter
D_d	droplet size
f_s	spacing of the fringe lines in the measurement volume
k_{droplet}	thermal conductivity of the droplet
k_{gas}	thermal conductivity of the gas medium
I	mass flux out of the droplet
j	mass flux of vapor
L	latent heat of vaporization
m	mass of the droplet
Nu	Nusselt number
P	total gas pressure
p_s	partial pressure of the vapour at the surface

q	heat flux
Q	heat flux out of the droplet
R_0	initial droplet diameter
Re	Reynolds number
Sc	Schmidt number
τ_L	lifetime of the droplet
$t_{\text{transient}}$	transient time period
T	temperature
U_D	droplet velocity
V	droplet volume
α	thermal diffusivity
β	geometrical factor
η	the refractive index of the continuous phase
λ	laser light wavelength
μ_{gas}	viscosity of the gas surrounding the droplet
v_{rel}	relative velocity between the droplet and the gas
ρ_{gas}	density of the gas
τ	representative timescale over which evaporation occurs
τ_D	frequency of the Doppler burst signal
Φ	Doppler burst phase shift

1. INTRODUCTION

1.1 Background Information

Aerosols are widely used in the medical field for the treatment of lung diseases since they are a convenient way for localised delivery of liquid or solid drugs to the lung. For applications in treating diseased lungs, localised drug delivery is advantageous since the drug takes effect more rapidly and with reduced side effects compared to systemic delivery methods. Thus, although medical aerosols have some disadvantages (e.g. deposition of drug on the mouth and throat, a variable and unpredictable dose, and ineffective drug delivery in lungs that are severely obstructed), they are the method most widely used to deliver drugs for the treatment of asthma and other lung diseases. There are three common ways of generating medical aerosols; nebulizers, metered dose inhalers, and dry powder inhalers.

Nebulizers

There are two main classes of nebulizers : jet nebulizers and ultrasonic nebulizers. The basic mechanism behind the operation of jet nebulizers is the atomisation of the medicine solution through the use of a venturi nozzle, where the liquid is drawn into an air jet, which entrains the liquid, stretching the liquid filament until instability is reached and the liquid breaks up into droplets. Ultrasonic nebulizers make use of piezoelectric crystals to generate high frequency vibrations, which are transmitted through a coupling fluid to the solution being

nebulized. The vibrations create a fountain of liquid from which a cloud of small droplets are continuously emitted.

Metered Dose Inhalers

Metered Dose Inhalers (MDI's) have two main parts : a small pressurized aluminium canister and a plastic actuator. The aluminium canister is filled with drug formulation, either with drug dissolved in a propellant or with milled micron-sized drug particles suspended in a propellant mixture. MDI's generate aerosols through the flash evaporation of the propellant contained in the drug formulation. When the MDI is actuated, the drug mixture contained in the metering chamber is released through the valve stem of the MDI into an expansion chamber in the actuator piece. Here, the fluid is not in a stable state of thermodynamic equilibrium (i.e. it is metastable). The fluid then flows through the actuator nozzle, as a metastable multiphase flow, where close packed arrays of bubbles form and move downstream. The bubble cloud moves and expands downstream due to the turbulent motion of the fluid, where the bubbles then come into contact with each other and explode, atomizing the bulk fluid. This flow usually proceeds out of the nozzle at a high velocity, ~50m/s.

There are also devices available which correct some of the problems associated with using MDI's. Usually referred to as spacers, these are holding chambers for the aerosols emitted from the MDI. The use of a holding chamber with an MDI has two main effects: 1) the larger particles are removed through impingement on the

walls of the chamber, and 2) the average velocity of the aerosol plume is significantly reduced. These two factors both serve to decrease oropharyngeal deposition and to increase the respirable fraction of the aerosol. Spacers also remove the need for the patients' coordination of their breath inhalation with the MDI actuation.

Dry Powder Inhalers

Dry powder inhalers (DPI's) were developed to provide the same convenience of MDI's, but without the environmentally damaging fluorocarbon propellants. DPI's use a system where the user's breath intake either generates turbulence or makes a turbine rotor spin, which then dispenses pre-powdered drug particles into the air stream. The powdered drug is either scraped off a compressed block of micronized drug, released from capsules containing the drug, or released from a small aluminium blister, several of which are located on a disk, each containing a specified amount of powdered drug. In order for some types of DPI's to function effectively, high inspiratory flowrates are required. This may cause reduced therapeutic benefits for patients not able to generate the high flowrate. The high flowrate also causes high oropharyngeal deposition, comparable to the levels that result from the use of MDI's.[1-4]

The three different types of aerosol generation devices each have applications where they are most effective. Due to the bulk of the air compressor or power transformer, nebulizers are not suitable when portability is required.

However, nebulizers are the most practical method of medical aerosol delivery for high dosage amounts, and are also well suited for delivering aerosols to infants and other patients who either cannot generate the required flow rate for using DPI's or are able to provide the level of co-ordination and cooperation required to use MDI's.

DPI's and MDI's have similar characteristics, both being small and portable. They are ideal for the treatment of asthma, the onset of which might occur at anytime, since they are easy for the patient to carry around wherever they go. The choice between a MDI and a DPI would depend on several factors, such as the patient's ability to achieve the flowrate required for the effective usage of a DPI, the type of medication being administered (as some medical formulations are more stable as a solid), and the severity of the side-effects caused by oropharyngeal deposition (a MDI with a spacer might lead to less oropharyngeal deposition than a DPI). Except in the case of the dry powdered inhaler where the powdered drug is scraped off a block of drug, DPI's generally do not carry as many doses as MDI's. However, many DPI's are easily refillable. The refillings are usually accomplished simply by inserting a disk with drug blisters or capsules.

MDI's might also be more convenient for the patients as they can hold up to 200 doses and do not require frequent refilling like many DPI's. Presently, MDI's are the most widely used aerosol delivery system in the medical field due to their portability and convenience of use.

1.2 Research Objectives

This research is targeted towards the improvement of modelling the deposition of MDI's in the lung. It will provide a measure of the accuracy of the current evaporation model used. Thus a more accurate aerosol evaporation theory, the topic of future study, will yield a more accurate lung deposition model when dealing with MDI's.

2. EXPERIMENTAL METHODOLOGY

2.1 Experimental Apparatus

2.1.1 Stage

The apparatus used in this research consists of 2 main sections : the stages and the modified MDI canister. The two part tri-axial stage is fastened to the support structure of a Dantec PDA (Phase Doppler Anemometer) laser measurement system. The primary stage, shown in Figure 2.1, is a 50 cm long uni-directional stage that moves the MDI along the axis of the plume. The secondary stage, shown in Figure 2.2, is a bi-directional stage that moves that MDI across the cross-section of the plume. The primary stage allows a 30 cm range of motion, and does not have a pre-fabricated scale. The secondary stage allows 10 cm of vertical movement and 6 cm of horizontal movement, and has a built in scale which reads 0.1 mm. The primary stage's main function is to allow measurements to be taken at different distances from the nozzle of the MDI along the center of the plume, and the secondary stage allows the MDI and the laser to be aligned such that the measurements are done at the center-line of the spray. The center-line of the spray was determined both from locating the point of maximum velocity across the plume and through visual inspection.

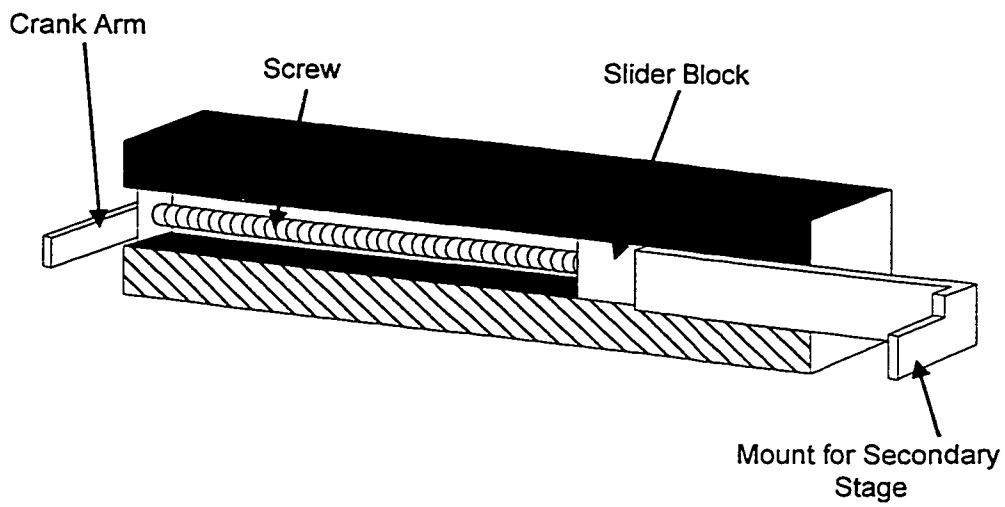


Figure 2.1 : Primary Stage

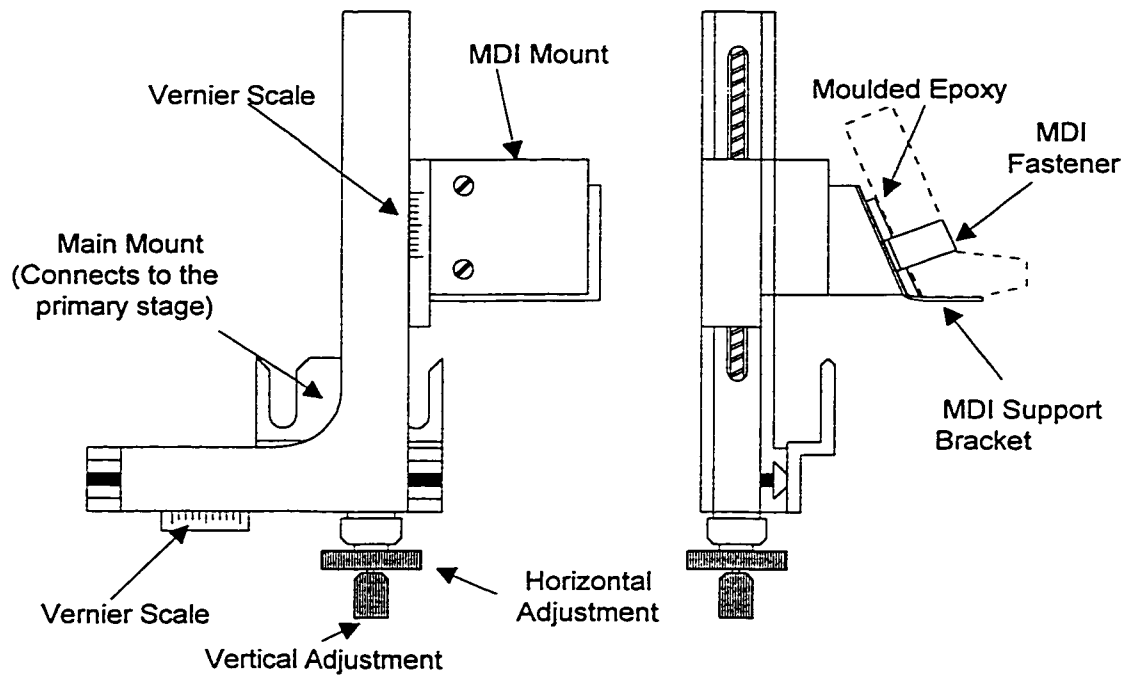


Figure 2.2 : Secondary Stage

2.1.2 Modified MDI

The MDI used is a standard MDI canister connected to various measurement and control devices and modified to allow quick refilling. It was found that temperature modulation was necessary as the characteristics of the particles ejected from the MDI were dependent upon the temperature of the canister, and each actuation lowered the temperature of the MDI canister.

It was noticed that if the MDI was fired repeatedly, with only a one second pause between the actuations, the aerosol sizes slowly increased and the velocity decreased with the cooling of the canister, until a steady state temperature was reached. Thus, in order to reflect the normal conditions under which MDI's are used, which is one or two actuations at each use, the MDI being measured has to be kept at a consistent temperature while measurement takes place. A small heat exchanger, a wound copper tubing, was therefore connected to the canister, and a constant temperature water bath was used to regulate the temperature of the water flowing through the heat exchanger. The water bath was then set to ambient temperature to speed up the return of the canister temperature to ambient temperature. This usually took 1 to 2 minutes. To further increase the speed at which the MDI reached ambient conditions after each firing, a film heater was attached the canister. This was activated for brief periods of time after actuation of the MDI, to add more heat to the system. A thermocouple was also attached to the canister to facilitate continuous monitoring of the temperature of the canister.

The canister itself had been specially modified to allow quick and easy recharges. A small hole with a diameter of approximately 1mm was drilled through the wall of the canister. A metal collar fitted with a valve was fastened over the hole, and an o-ring was used to seal the joint between the valve and the hole. The MDI was then refilled with Freon 12 from a storage cylinder, as needed. The modified canister, as described above, removed the need to refill empty MDI canisters. Figure 2.3 shows a schematic of the MDI modified with the metal collar and the wound copper heat exchanger.

The refilling of the MDI was accomplished by cooling the canister down to -40°C , using dry ice, and then connecting the MDI to a tank containing Freon 12. After five minutes the MDI was removed from the dry ice and allowed to slowly return to ambient temperature. The MDI remained connected to the freon tank as it returned to ambient temperature to ensure that the canister was not over-pressurised. The canister was then fired ten times before measurements were taken, to bleed of possible excess pressure.

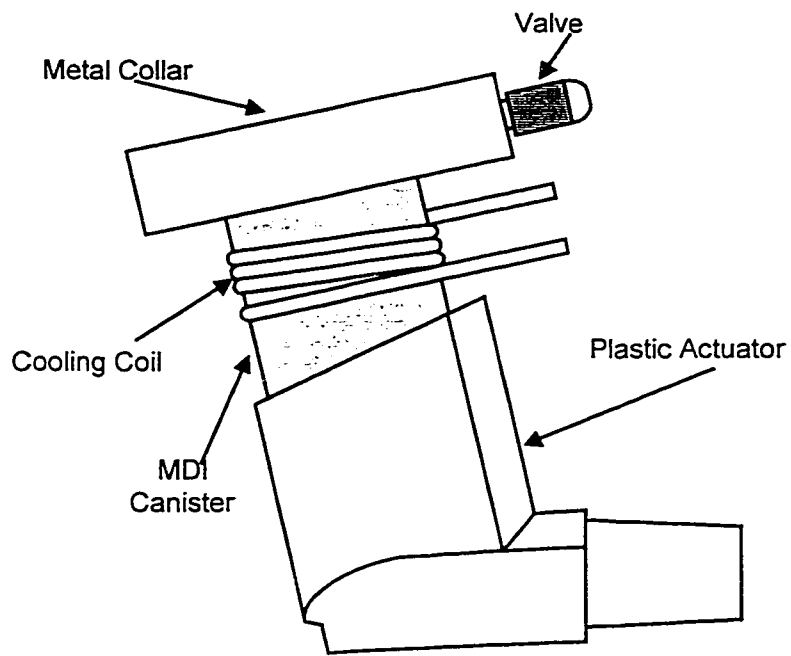


Figure 2.3: Modified MDI Canister

2.2 Measurement of Particle Velocity and Size Distributions

A regular drug formulation was not used in this study as it was difficult to estimate what effects the surfactants and other compounds in the formulation had on the evaporation rate of Freon 12. The experiments were thus conducted with pure propellant, which meant that given time the particles would evaporate completely. This made the use of a cascade impactor or other such non-instantaneous particle diameter measuring devices impractical. Phase doppler anemometry is desirable in this situation as it measures both the velocity and the size of particles without causing disturbances to either characteristic.

2.2.1 Theory of Operation of the PDA

The Dantec PDA measures particle size and velocity by detecting the Doppler shift and frequency of laser light scattered by a moving object, in this case Freon 12 aerosol droplets moving in air.

In the optical system of the PDA, a laser beam is split into two beams that intersect and form a fringe pattern. The intersection of these two beams form the measurement volume. When a particle passes through the measurement volume, light is scattered. This light is focused onto a photo-detector, generating a Doppler burst signal. This signal provides the information required to calculate drop velocity, size, and concentration.

Since the frequency of the Doppler burst is dependent on the fringe spacing in the measurement volume and the velocity of the particle, the droplet velocity is then obtained from the Doppler burst signal frequency using

$$U_D = \frac{f_s}{\tau_D}$$

where U_D is the droplet velocity, f_s is the spacing of the fringe lines in the measurement volume, and τ_D is the frequency of the Doppler burst signal. To obtain the particle size, a second detector is added to the system a fixed distance away from the first detector. A phase shift is introduced to each of the signals when the drop interference fringe pattern is focused onto the second detector, and the phase shift can be related to particle size using geometrical optics theory. It should be noted that this is only valid for spherical droplets. When the receiving optics are arranged at an off-axis orientation known as the optimum scattering angle, there is a linear relationship between the particle size and the Doppler phase shift, given by the equation

$$D_d = \frac{1}{2\beta} \left(\frac{\lambda_0}{\pi\eta} \right) \Phi$$

where D_d is the droplet size, Φ is the Doppler burst phase shift, λ is the laser light wavelength, η is the refractive index of the continuous phase, and β is a geometrical factor that is dependent on the light scattering mechanism and the optical configuration of the instrument. Expressions for β can be found in [5].

A third detector is present in the system to increase the dynamic particle size measurement range, and to validate particle sphericity. [6,7]

2.2.2 Configuration of the PDA

The following is a description of the configuration of the Dantec PDA system, with a 9055X4681 transmitting optics, a 9057X0103 receiving optics and a 58N10 signal processor. The PDA is set-up to measure refracted light.

The fringe spacing is $2.6697\mu\text{m}$ using the current set-up, with 75 fringes in the measurement volume.

A 36Mhz band pass filter was used on the Doppler signals, in order to accommodate the high particles velocities (Max. of $\sim 45\text{m/s}$) measured.

The data is acquired and processed through Dantec's SIZEware software, Version 2.1.

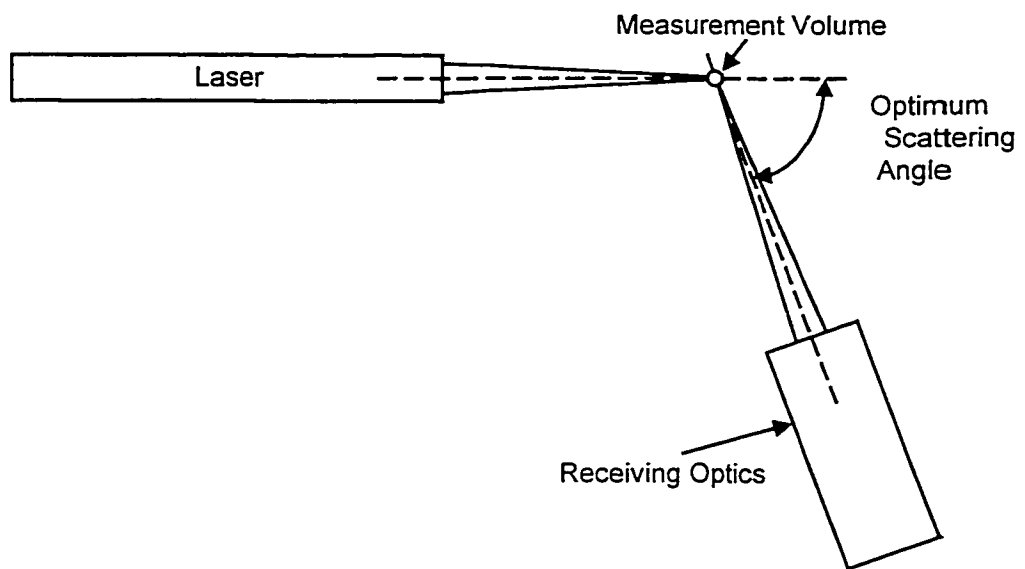


Figure 2.4 : Dantec PDA Schematic

2.2.3 Measurement Procedure

The measurement procedure is as follows; at the start of every day of measurement, the laser was adjusted and focused. A visual inspection was then done to ensure that the canister was positioned such the measurement volume of the laser was aligned with the center of the plume. This was done by firing the MDI repeatedly and making sure that the laser beams from the Dantec PDA system intersected at the center of the plume. The canister was then allowed to return to ambient temperature, hastened by brief periods of heating. The data collection program was then started, and the MDI was moved to the desired distance away from the laser. The MDI was then actuated and brought back to ambient temperature. This was repeated thirty times for each run, and ten runs were done for each measurement location.

The measurements were taken at the following distance away from the nozzle: 0.4 cm, 2.4 cm and 4.4 cm. The data output consists of the velocity and the mass of the particles that passed through the measurement volume. No further measurements were taken as the laser did not reliably detect particles beyond 4.4 cm, yielding very low validation rates and detecting very few particles, in the order of 100. This was probably due to the particles being too dispersed for the laser to detect and to provide a meaningful output.

The data from the 10 runs were then collated and averaged, to yield the average velocity and the averaged particle size distribution over 300 measurements at each measurement location.

3. THEORY OF DROPLET EVAPORATION

3.1 Assumptions Required

Currently, the theory most widely used in predicting aerosol particle size change is the classical theory of aerosol evaporation, a theory that views diffusion as the primary facilitator for aerosol size change. The classical theory will now be developed, and the assumptions required for the theory to be valid. This is a well known theory originated by Maxwell [8].

The following assumptions are made in the classical aerosol evaporation theory.

- 1. Mass transfer at the droplet surface does not cause any bulk motion in the air**

This implies that Stephan flow is neglected, which is the flow that occurs when a droplet evaporates at such a high rate that the vapour coming off the droplet sets up motion in the air surrounding the droplet.

According to N.A. Fuchs, 1959 [9], this assumption requires that the partial pressure of the vapour at the surface, p_s , is much less than the total gas pressure there, P , i.e. $p_s \ll P$.

- 2. The temperature is spatially uniform inside the droplet (lumped capacitance assumption)**

Thermodynamics show that in order for this assumption to be true, the ratio of the resistance to heat transfer within the droplet to the resistance to heat transfer at the droplet surface must be small [10]. For liquid droplets in gaseous media, this ratio, known as the Biot number, can be shown to be proportional to the Nusselt number times the ratio of the thermal conductivity in the gas surrounding the droplet to that in the droplet, i.e.

$$Bi = Nu \frac{k_{gas}}{k_{droplet}} \quad (3.1)$$

The Nusselt number, Nu, is a non-dimensional measure of the temperature gradient at the droplet surface. For a stationary sphere in quiescent fluid, Nu has a value of 2. Therefore, in order for the lumped capacitance assumption to be valid, i.e. have $Bi \leq 0.1$, for a stationary droplet in air, the following inequality must hold true

$$\frac{k_{gas}}{k_{droplet}} < 0.05 \quad (3.2)$$

3. Quasi-steady assumption

This assumption states that $\frac{dm}{dt}$ is small enough such that the heat and mass transfer rates of the droplet at an instant in time is the same as that of a droplet that is being maintained at that instantaneous radius. Perturbation analysis show that the steady state solution can be viewed as the zeroth order term of a perturbation

series, and if the higher order terms of the series are small, the steady state solution would be accurate. For this to be true, the following conditions are necessary ;

1. The density of the vapor phase at the droplet surface must be much less than

the density of the droplet, i.e. $\frac{c_s}{\rho_{drop}} \ll 1$.

2. $\frac{D\tau}{R_0^2} \gg 1$ and $\frac{\alpha\tau}{R_0^2} \gg 1$,

where D is the diffusion coefficient of the vapor in air, α is the thermal diffusivity of the gas surrounding the droplet, τ is the representative timescale over which, in our case, evaporation occurs and R_0 is the initial droplet diameter.

4. The vapor concentration and the gas temperature are functions only of distance from the center of the droplet.

For this assumption to be true the droplet cannot be moving through the gas at significant speeds. Thus only for a stationary droplet, or a droplet for which its Reynolds number approaches zero, is this assumption valid. The correction for any relative motion between the droplet and the surrounding gas will be small if the following inequality is true. [11]

$$0.6Re^{\frac{1}{2}}Sc^{\frac{1}{3}} \ll 2 \quad (3.3)$$

where Sc is the Schmidt number for the vapor in the gas surrounding the droplet and Re is the Reynolds number of the droplet. The Schmidt number and the Reynolds number of the droplet are given by the following expression ;

$$Sc = \frac{\mu_{gas}}{(\rho_{gas} D)}, \text{ and}$$

$$Re = \frac{v_{rel} \rho_{gas} d}{\mu_{gas}}$$

where μ_{gas} is the viscosity of the gas surrounding the droplet, ρ_{gas} is the density of the gas, v_{rel} is the relative velocity between the droplet and the gas, D is the diffusion coefficient of the gas, and d is the droplet diameter.

For air at room temperature, it can be shown that $Sc^{\frac{1}{3}}$ is generally of order one, therefore the inequality reduces to

$$Re^{\frac{1}{2}} \ll \frac{2}{0.6}$$

$$Re \ll 10 \quad (3.4)$$

Therefore, for assumption 4 to be valid, the particle Reynolds number must be less than or equal to one.

5. The particle radius must be much greater than mean free path of the gas surrounding the droplet.

This requirement stems from the fact that if the droplet radius approaches the mean free path of the gas, the continuum assumption at the droplet surface, used to develop the classical theory, breaks down. For pharmaceutical aerosols however, assumption 5 is generally valid as droplets with radii that are close to the mean free path carry an insignificant amount of drug, and thus are not important. In the case of this particular experiment, the lower bound of the Dantec PDA measurement capabilities is a particle size of around 0.5 μm , and most of the particles are of the order of 10 μm . Thus, since the typical value of the mean free path of air is approximately 0.07 μm , the assumption of particles radius \gg mean free path is valid for this application.

3.2 Classical Theory

Assuming that the total density of the gas is independent of r (a reasonable assumption since the amount of vapor present is very small compared to the amount of air around the droplet and assumption 1 above requires $p_s \ll P$), Fick's first law of diffusion gives

$$j = -D\nabla c \quad (3.5)$$

where j is the mass flux of vapor, D is the diffusion coefficient of the vapor in air, and c is the density of the vapor. Taking into account that only radial variance of

properties was assumed, the equation can be rewritten as

$$j = -D \frac{dc}{dr} \quad (3.6)$$

Thus the mass flux through a sphere circumscribing the droplet at radius r would be given by mass flux j multiplied by the surface area of the sphere, which yields

$$I = -4\pi r^2 D \frac{dc}{dr} \quad (3.7)$$

Applying mass conservation, under steady state conditions, I must be independent of r . Equation (3.7) can be written as

$$\frac{dc}{dr} = -\frac{I}{D4\pi r^2} \quad (3.8)$$

If there are no large temperature gradients in the gas near the droplet, then a constant diffusion coefficient can be assumed. Integrating with respect to r from the droplet surface to infinity gives

$$c_s - c_\infty = \frac{I}{2\pi dD} \quad (3.9)$$

which can be rewritten as

$$I = 2\pi dD(c_s - c_\infty) \quad (3.10)$$

Since I is equivalent to the mass flux out of the droplet, one can write

$$I = -\frac{dm}{dt} \quad (3.11)$$

Thus, the equation that governs the rate of change of mass of the droplet is

$$\frac{dm}{dt} = -2\pi r D(c_s - c_\infty) \quad (3.12)$$

Similarly, by following the same steps, the governing equation for the temperature of the droplet can be derived. Fourier's law gives the heat flux at any point as

$$q = -k\nabla T \quad (3.13)$$

where q is the heat flux, k is the thermal conductivity of the gas surrounding the droplet, and T is the temperature of the droplet. Based on the requirement that $p_s \ll P$, one can use $k = k_{\text{air}}$, as the amount of vapor is too little to significantly change k . Also, k is approximately constant in the temperature range the droplet will experience.

Assuming that conduction is the only significant mode of heat transfer, in accordance with assumption one, convection is negligible. Also, as Fuchs 1959 [9] shows, radiative heat transfer is negligible. Once again, since properties only vary radially, one can write

$$q = -k \frac{dT}{dr} \quad (3.14)$$

The energy flux out of a sphere with radius r around the droplet is q multiplied by the surface area, i.e.

$$Q = -4\pi r^2 k \frac{dT}{dr} \quad (3.15)$$

With the quasi-steady assumption, Q must be independent of r , and thus, integrating with respect to r from the droplet surface to infinity yields

$$Q = 2\pi dk_{air}(T_s - T_\infty) \quad (3.16)$$

In order to complete this derivation, the energy balance for the droplet at an instant in time has to be considered. It is dependent on the following factors :

1. the rate of energy change due to heat conduction, Q ,
2. the rate of energy change due to energy removed by evaporating vapor, $L \frac{dm}{dt}$,

where L is the latent heat of vaporization of the liquid,

Combining the two would give the rate of energy change of the droplet,

$\rho_{drop} c_p V \frac{dT}{dt}$, where ρ_{drop} is the density of the droplet liquid, c_p is the heat capacity of the droplet liquid, and V is the droplet volume, $\pi \frac{d^3}{6}$.

This gives

$$L \frac{dm}{dt} + Q = \rho_{drop} c_p V \frac{dT}{dt} \quad (3.17)$$

Substituting the expressions for $\frac{dm}{dt}$, Q , and V into the equation, and noting that with the lumped heat capacitance assumption, $T = T_s$, the equation for the temperature of the droplet is obtained,

$$-LD(c_s - c_\infty) - k_{air}(T - T_\infty) = \frac{dT}{dt} \rho_{drop} c_p \frac{d^2}{12} \quad (3.18)$$

The solution to this equation is obtained by simultaneously solving the rate of mass transfer equation, and using an equation that relates c_s to T . Generally, the RHS of the equation is neglected, as shown below. In order to compare the magnitudes of the terms in the equation, the equation should be nondimensionalized. To accomplish this, the following non-dimensional variables were introduced:

$$T^* = \frac{(T - T_\infty)}{\Delta T}, \text{ where } \Delta T \text{ is some characteristic temperature difference,}$$

$$c^* = \frac{(c_s - c_\infty)}{\Delta c}, \text{ where } \Delta c \text{ is some characteristic concentration difference,}$$

$$d^* = \frac{d}{d_0}, \text{ where } d_0 \text{ is the initial droplet diameter,}$$

$$t^* = \frac{t}{t_L}, \text{ where } t_L \text{ is the droplet lifetime.}$$

Putting these new variables into the equation gives,

$$(D\Delta c)c^* + (k_{air}\Delta T)T^* = -\left(\frac{\rho_{drop}c_p\Delta Td_0^2}{12t_L}\right)d^{*2}\frac{dT^*}{dt^*} \quad (3.19)$$

Thus the RHS of the equation will be negligible if $\left(\frac{\rho_{drop}c_p\Delta Td_0^2}{12t_L}\right)$ is much less than either of the two coefficients on the LHS of the equation. Comparing it to the coefficient of the nondimensionalized temperature term, requires that

$$\left(\frac{\rho_{drop}c_p\Delta Td_0^2}{12t_L}\right) \ll k_{air}\Delta T \quad (3.20)$$

This simplifies to

$$\left(\frac{\rho_{drop} c_p d_0^2}{12 t_L k_{air}} \right) \ll 1 \quad (3.21)$$

In order to evaluate this inequality, an expression for the droplet lifetime is required. The droplet lifetime can be estimated by going back to (3.18) and assuming that $\rho_{drop} c_p \frac{d^2}{12} \frac{dT}{dt}$ is indeed negligible. This might seem a circular argument, but this is neglected only to obtain an estimate of the droplet lifetime. Thus, an equation for droplet temperature reduces to

$$LD(c_s - c_\infty) + k_{air}(T - T_\infty) = 0 \quad (3.22)$$

This is an algebraic equation with T as the only unknown, since L, D, k_{air} , c_∞ and T_∞ are all known quantities, and c_s is a function of T. This also implies that the temperature of the droplet remains constant throughout the process of evaporation. T can then be obtained by solving the equation iteratively. Knowing that

$\frac{dm}{dt} = \rho_{drop} \pi \frac{3d^2}{6} \frac{dd}{dt}$, the mass transfer rate equation can be rewritten as

$$\frac{dd}{dt} = \frac{4D(c_s - c_\infty)}{\rho_{drop} d} \quad (3.23)$$

and $\frac{dd}{dt}$ can be solved as c_s can be found from the T found earlier. For a single droplet evaporating in air, the ambient conditions, c_∞ and T_∞ are assumed constant, i.e. the mass and heat transfer from the droplet to the environment are small enough such that there are no significant changes to the ambient conditions.

Also, for a pure substance c_s is only dependent on T , thus a constant droplet temperature implies a constant vapor density at the surface of the droplet.

Thus equation (3.23) can be integrated with respect to time to obtain

$$d_0^2 - d^2 = \frac{8D(c_s - c_\infty)}{\rho_{drop}} t \quad (3.24)$$

Here, d_0 is the initial droplet diameter.

To find how long it takes the droplet to completely evaporate, the droplet lifetime, one would set d as zero, and find t . Thus,

$$t_L = \frac{\rho_{drop} d_0^2}{8D(c_s - c_\infty)} \quad (3.25)$$

This is substituted back into the inequality (3.21), and one obtains

$$\frac{2D(c_s - c_\infty)c_p}{3k_{air}} \ll 1 \quad (3.26)$$

If this inequality is true, the RHS of equation (3.19) can then be neglected, and the droplet temperature remains constant throughout the process.

However, there is a transient portion while the temperature of the droplet changes from its initial temperature to its steady-state temperature. During this time, one needs to determine if $\frac{dT}{dt}$ is large, which could cause the RHS of the equation to be significant in this time period. Assuming that during the transient period any heat transfer taking place is balanced by an energy change in the

droplet, with no mass transfer, the equation now becomes

$$-k_{air}(T - T_{\infty}) = \rho_{drop} c_p \frac{d^2}{12} \frac{dT}{dt} \quad (3.27)$$

For a temperature change of ΔT (i.e. $T - T_{\infty}$) to occur in a time of Δt , the equation

suggests that $-k_{air}\Delta T \approx \rho_{drop} c_p \frac{d^2}{12} \frac{\Delta T}{\Delta t}$

This then gives

$$\Delta t \approx \rho_{drop} c_p \frac{1}{k_{air}} \frac{d^2}{12} \quad (3.28)$$

Here, Δt represents the transient time period, and comparing it to the droplet life time, the following equation is obtained

$$\frac{t_{transient}}{t_L} = \frac{3Dc_p c_s}{4k_{air}} \quad (3.29)$$

Thus, if $\frac{t_{transient}}{t_L} \leq 0.1$, the transient time period would be of a short enough duration

when compared to the lifetime of the droplet that the RHS of the equation can be neglected.

In conclusion, in its simplified form, the classical theory of aerosol evaporation yields the following as governing equations

$$\frac{dm}{dt} = -2\pi dD(c_s - c_{\infty})$$

$$LD(c_s - c_{\infty}) + k_{air}(T - T_{\infty}) = 0$$

which require the assumptions discussed earlier in the chapter to be valid. These equations are then solved with an equation relating c_s and T .

4. RESULTS AND ANALYSIS

4.1 Computer Code

A computer code which used the classical theory to predict the size changes experienced by a pure Freon 12 aerosol generated from an MDI was written, and the following describes the details of the code. A line listing of the code is provided in the appendix. Since the purpose of this thesis was to predict the size change of the droplet rather than the initial size of the droplet, the particle sizes and velocities at the first data measurement point are taken and used as a starting point for the code. The data collection program that the Dantec PDA utilises has as output the particle size distribution, where the number of particles in 0.3 μm and 0.2 μm size bins and the corresponding average velocity of the particles in that size class are shown. The size bins are examined individually using the computer code, and the size change for the particles in a size class based on the median diameter of the bin range is then calculated.

The measured velocities of each size bin are number averaged, and a curve is fitted over the velocities at the 3 measurement locations, to obtain an approximate relationship between the average velocity of the particles and the distance from the nozzle. The velocity-distance relationship is only a crude approximation, because the different sized particles have different velocities, and hence evaporate to different degrees when they reach the measurement points. However, due to the particles switching to lower size bins as they evaporate, it is

very difficult to track a particular size class through its size changes and hence its velocity from the PDA data. This velocity curve is used to compute the time it takes for the particles to travel from one measurement point to the other, and the time thus obtained is used to calculate how much the droplet evaporates when it gets to the next measurement point. This information is then compared to the experimental data.

The experimental data was generated by averaging the data obtained from the ten runs at each measurement location. The output from the PDA data acquisition program was read into an excel spreadsheet, and the average velocity at each size bin was calculated. The results were then output in Lotus® spreadsheet format, and read into the computer code.

To obtain the relationship between the droplet surface concentration of freon and the temperature, empirical equations of state were used. The equations provided a way to calculate the vapor pressure of freon at the surface of the droplet, which was then converted to concentration using the ideal gas law, which gives

$$c_s = \frac{P}{RT} \quad (4.1)$$

where P is the vapor pressure, R is the gas constant, and T is the temperature of the Freon 12, in kelvin.

4.2 Results and Analysis

The following results were obtained using the computer program and through experiments. Figure 4.1, 4.3 and 4.5 shows the theoretical and experimental particle mass distributions at 0.004 m, 0.024 m and 0.044 m away from the mouthpiece of the MDI respectively. Figures 4.2, 4.4 and 4.6 show both the theoretical and experimental cumulative particle mass distribution at 0.004 m, 0.024 m, and 0.044 m from the end of the mouthpiece, respectively. Figures 4.1 and 4.2 show no difference between the theoretical and experimental results as the experimental results at 0.004 m are used as the starting point for the computer code. The MMD (Mass Median Diameter) and GSD (Geometric Standard Distribution) for both the theoretical and experimental curves is 8.85 μm and 1.39 respectively. Comparing the theoretical and experimental mass distributions in Figure 4.3, at 0.024 m, one can see that the portion of the theoretical curve with an aerodynamic diameter below 10 μm has shifted to the left, indicating that the number of smaller particles are increasing. The cumulative particle mass distributions on Figure 4.4 indicate a larger geometric standard deviation, 1.46 compared to an experimental GSD of 1.35. The MMDs are quite similar for the theory and experiment, 8.81 μm and 8.85 μm respectively. Figure 4.5 shows a more obvious shift towards the left for the theoretical mass distribution, for particles with an aerodynamic diameter less than 10 μm . The theoretical curve also shows higher particle mass fractions in some of the size bins between 10 μm

to 25 μm . This could be due to the merging of particles in different size classes into one size class as they evaporate, since the particles in the different size class are travelling at different velocities, leading to differing amounts of time elapsed as the particles travel from one point to the next. The merging of particles in the different size classes in the computer code is thus made possible. Again, Figure 4.6 indicates that theory predicts a larger GSD, 1.51, than the experimental GSD of 1.36, with a theoretical MMD of 9.55 μm and an experimental MMD of 9.35 μm .

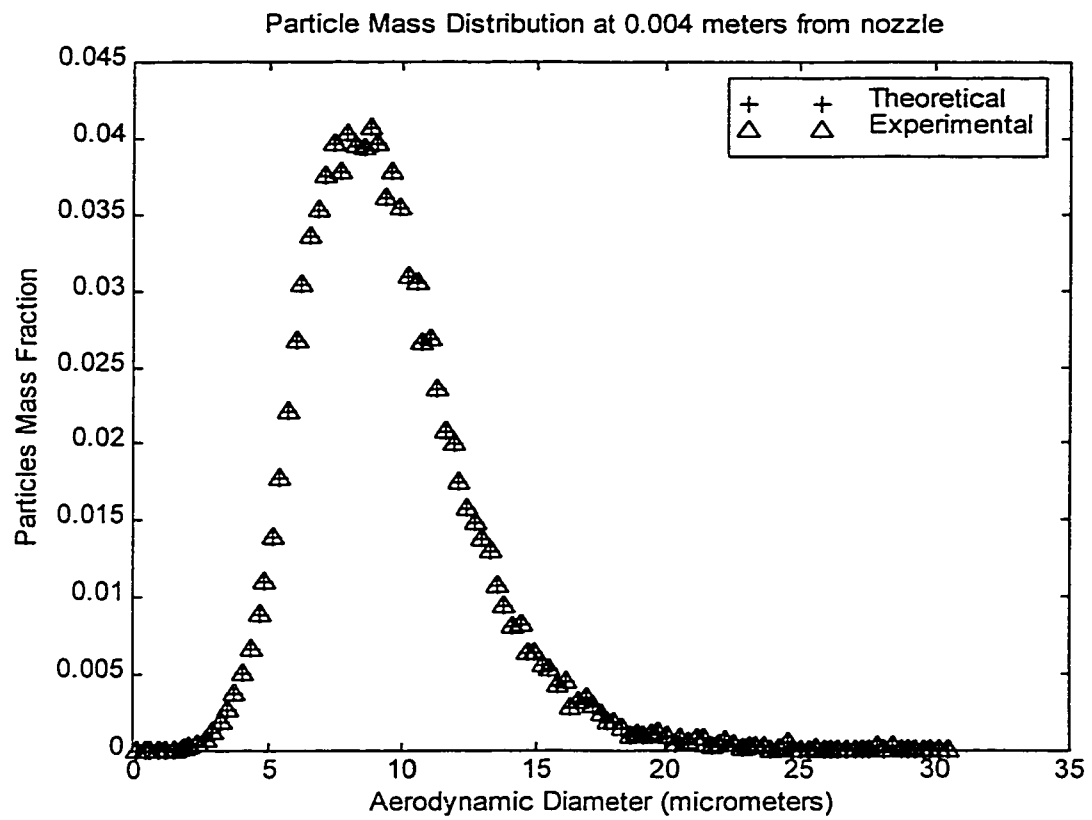


Figure 4.1 : Particle mass distribution at 0.004 m

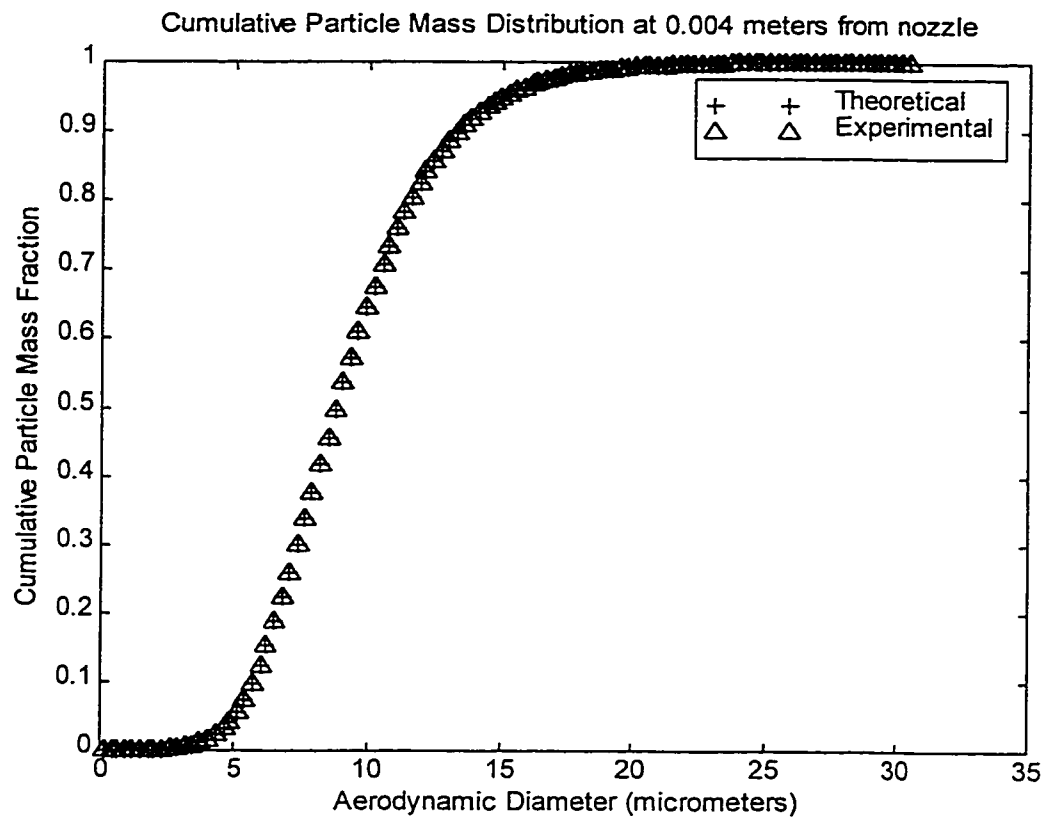


Figure 4.2 : Cumulative particle mass distribution at 0.004 m

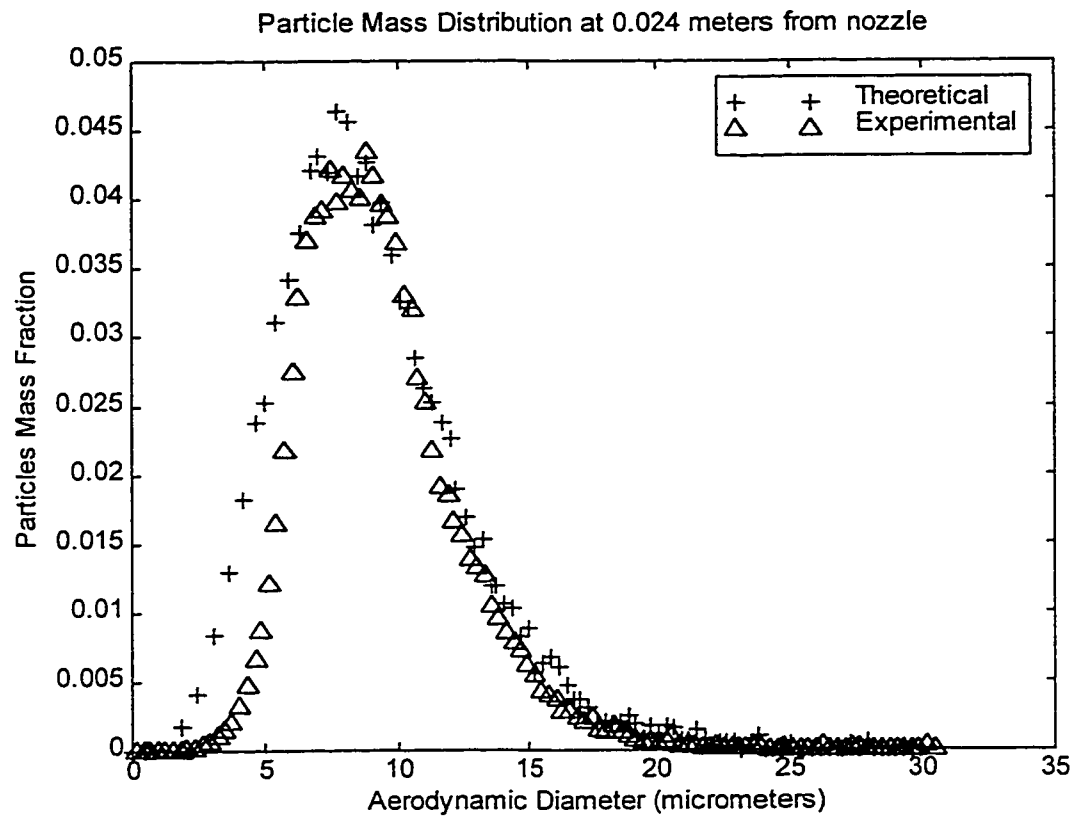


Figure 4.3 : Particle mass distribution at 0.024 m

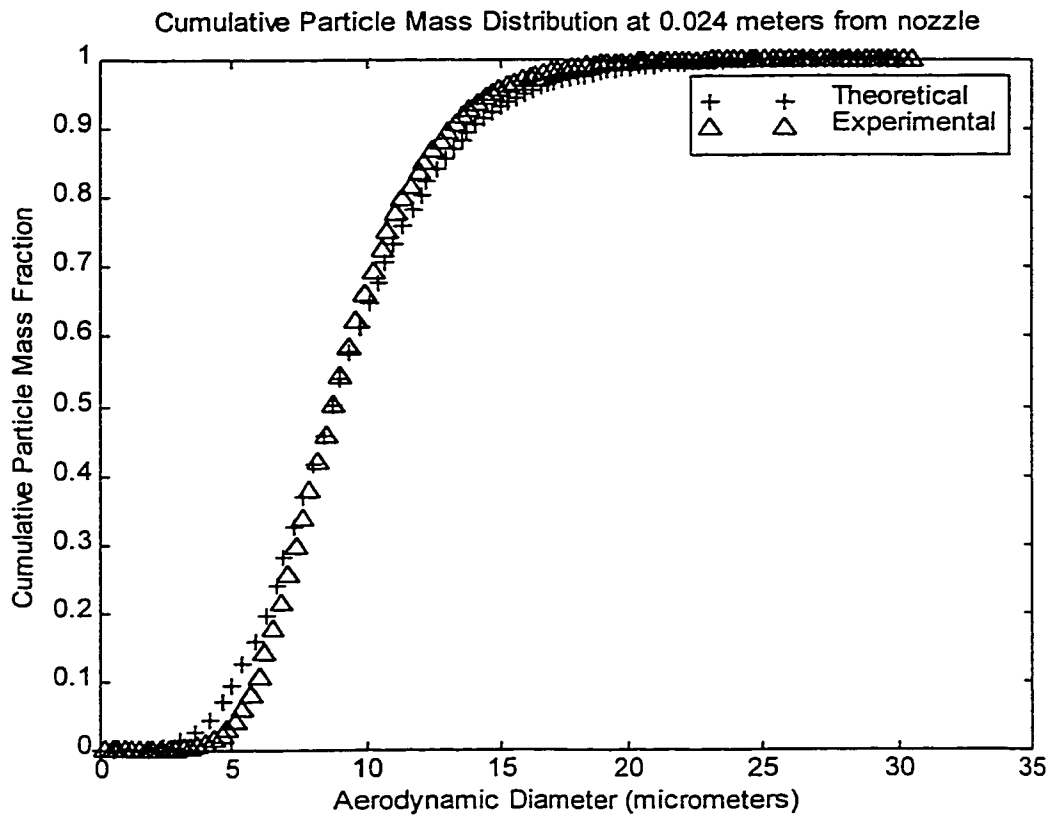


Figure 4.4 : Cumulative particle mass distribution at 0.024 m

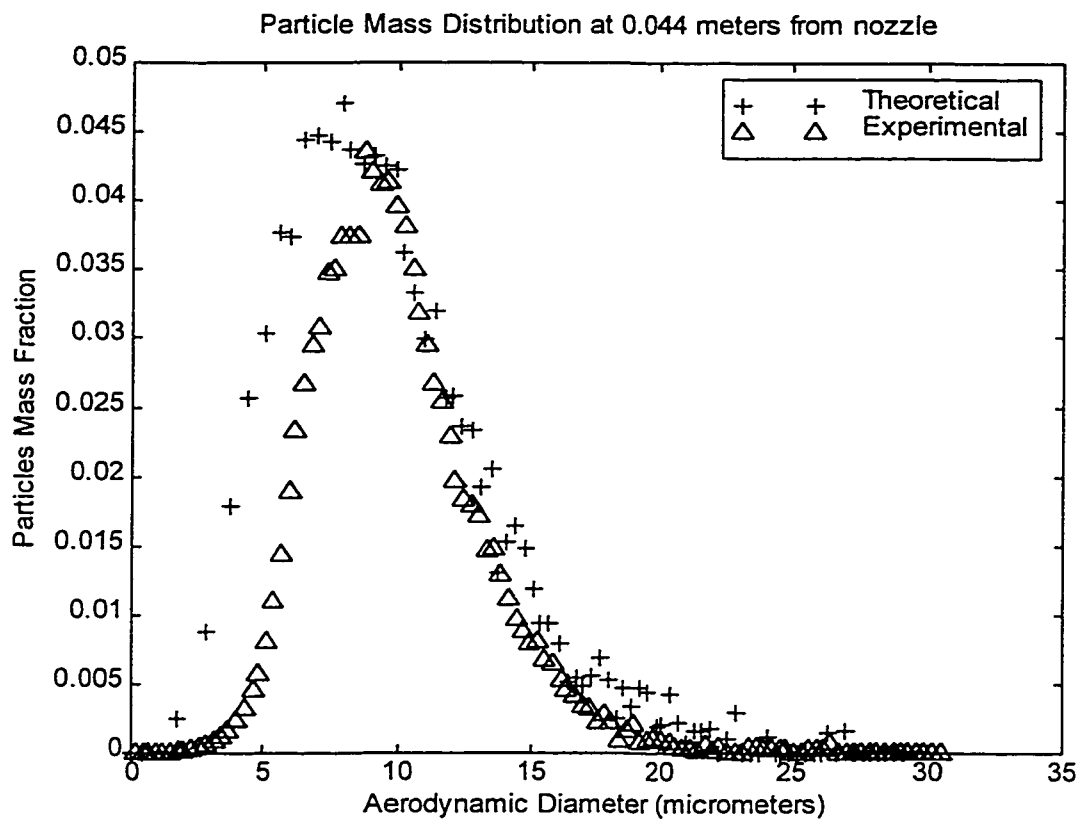


Figure 4.5 : Particle mass distribution at 0.044 m

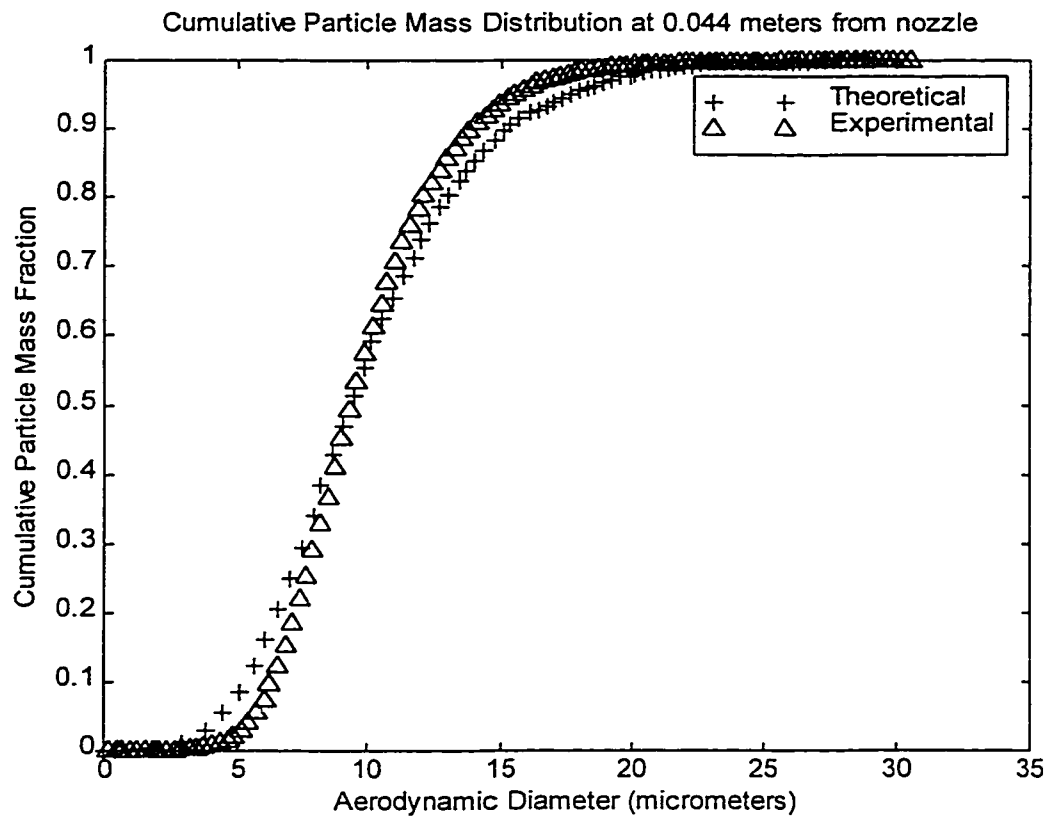


Figure 4.6 : Cumulative particle mass distribution at 0.044 m

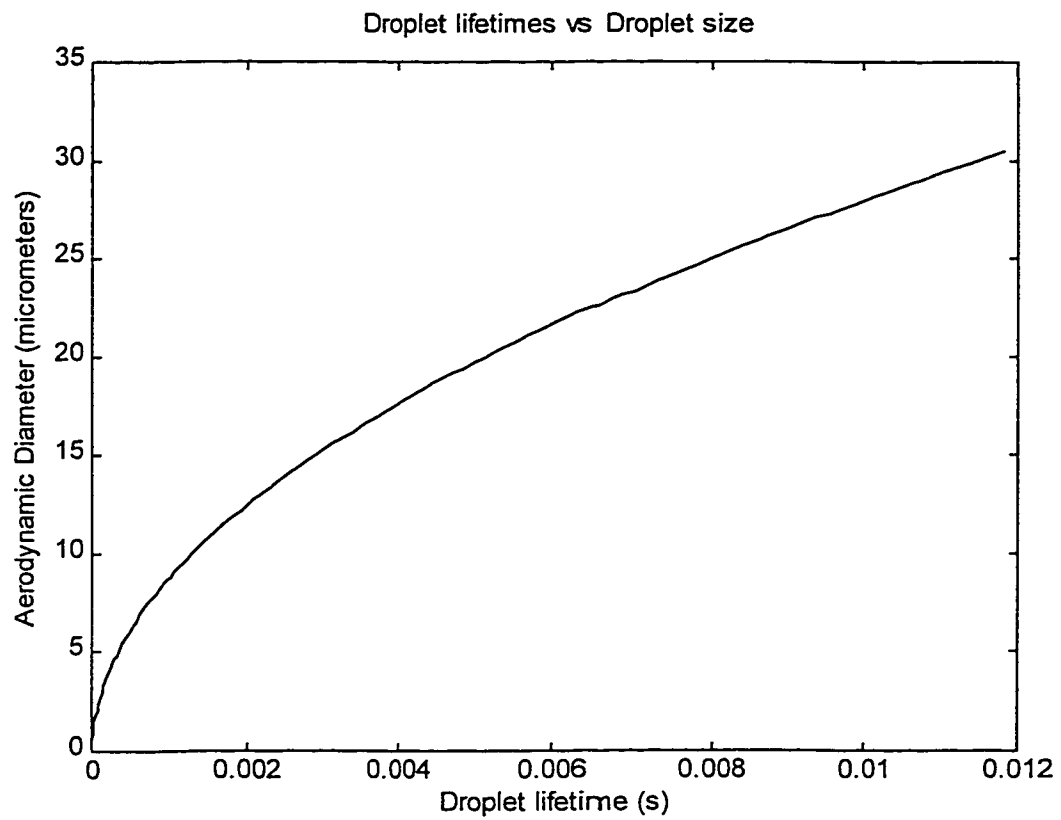


Figure 4.7 : Droplet lifetimes as predicted by classical theory

To get a better indication of how the droplets are evaporating, a plot of droplet sizes versus droplet lifetime was generated with the computer code, which is shown in Figure 4.7. As the figure indicates the relationship between droplet size and lifetime is quadratic, which is as expected for the classical theory.

4.3 Discussion of Results

Comparisons of the theoretical and experimental results indicate that the theoretical particle size change is greater than that found in experiment. One distinct trend that is evident in the cumulative mass distributions is that compared to experiments, theory predicts a larger number of small particles and a smaller number of large particles. This is in accordance with the theory over-predicting evaporation rates, which would “shift” more particles in the larger particle size range, 10 μ m - 30 μ m, into the smaller particle size range, from 0 μ m - 10 μ m.

The results show that the classical aerosol evaporation theory does over-predict the evaporation rates of propellant from aerosols generated by MDI's.

There are a few possible reasons for this.

1. Stefan flow might be an important factor in the evaporation of propellant from the droplets. In the experiment, the propellant droplets were entering an environment with a temperature 50°C more than the boiling point of Freon 12, and this would suggest that the droplets are evaporating rapidly, probably ejecting vapor at a rate that would make Stefan flow an important factor. The inclusion of

Stefan flow into the theory would serve to lengthen the droplet lifetimes, since Stefan flow is a flow of vapor out from the droplet. This means that heat now has to flow upstream against the Freon 12 vapor flow to reach the droplet. The rate of heat reaching the droplet is thus reduced, which then results in a decrease in the rate of evaporation of the propellant.

2. Another reason why the droplet lifetimes are underestimated by the theory is that the ambient concentration of Freon 12 vapor is assumed to be zero and ambient temperature is assumed to be room temperature. This however is most likely not the case in the aerosol plume. As the droplets in the aerosol plume evaporate, there is likely a concentration of Freon 12 vapor in the vicinity of the plume. Also, heat transfer between the aerosol and the environment might cause the air around the plume to be cooled down. Thus, the lack of two-way coupling in the code might account for some of the observed difference. Again, two-way coupling would serve to lengthen the theoretical droplet lifetimes. The presence of Freon 12 vapor in the aerosol plume would give a non-zero value for c_∞ , which would thus decrease the concentration gradient and reduce the mass transfer. Similarly, a cooler environment means a smaller temperature gradient, which lowers the heat transfer rate and ultimately the droplet evaporation rate.

3. Due to the low temperature of the Freon droplets, condensation of moisture in the air might increase the size of the droplets, and result in the experiment yielding a smaller evaporation rate when compared to theory.

4. The amalgamation of droplets might also be a factor in smaller observed evaporation rates when compared to theory.
5. The classical theory assumes that the temperature of the droplet is constant as it evaporates, due to the transient temperature term being negligible. This might not have been the case during the experiment, and a higher droplet temperature might have given smaller evaporation rates for the theory.

CONCLUSIONS

5.1 The Metered Dose Inhaler

The theory for predicting the evaporation rates of droplets generated by nebulisers is well-developed, allowing computer models to be created to facilitate in-vivo testing of nebulisers. This greatly speeds up the testing procedure by removing the need to involve a human subject. In-vivo testing also eliminates exposing a human subject to radiation, which in-vitro testing requires. An evaporation model that can be applied to MDI's would provide the basis of developing computer models to predict the deposition of MDI generated aerosol droplets in the lung, and greatly aid in the testing of MDI's.

5.2 Classical Droplet Evaporation Theory

The classical droplet evaporation theory predicts the evaporation rates of droplets based on the following five assumptions :

1. No Stefan flow
2. Temperature inside the droplet is uniform(Lumped heat capacitance)
3. The evaporation process is quasi-steady
4. The problem is one dimensional, i.e. vapor concentration and temperature of the gas medium are functions of radial distance only
5. The particle radius is much greater than the mean free path of the gas molecules

It was found that the classical evaporation theory over-predicted the evaporation rates of the droplets, yielding cumulative particle mass distributions that indicate theory predicts a larger number of particles in the $0\mu\text{m} - 10\mu\text{m}$ range, and a smaller number of particles in the $10\mu\text{m} - 30\mu\text{m}$ range when compared to experiments, which is indicative of a greater theoretical evaporation rate.

The classical evaporation theory is therefore not suitable for modelling the evaporation characteristics of aerosol droplets generated by MDI's.

5.3 Future Work

The effects of Stefan flow, which is a flow of vapor out of the droplet, could be included in the evaporation theory. Heat would have to flow upstream, against the flow of vapor, and thus the evaporation rate should be reduced. Two-way coupling could also be incorporated into the classical evaporation theory. This would account for the rise in concentration of vapor and a drop in temperature in the gas surrounding the droplet. This would reduce the concentration and temperature gradient, thereby reducing the evaporation rate. Also, further work needs to be done to investigate the effects of condensation of moisture, either on the particles or in the aerosol plume. The same experiment could be performed in dry air and the differences in the results, if any, could then be investigated.

REFERENCES

- [1] Thomas T. Mercer, "Production and Characterization of Aerosols", *Arch Intern Med.* Vol 131,1973.
- [2] Andrew R.Clark, "MDI's: Physics of Aerosol Formation", *Journal of Aerosol Medicine*, Volume 9, Supplement 1, 1996
- [3] "Aerosol Consensus Statement" *Respiratory Care*, Vol 36 No.9, September 1991.
- [4] C.A. Dunbar, A.P. Watkins, and J.F. Miller, "Theoretical Investigation of The Spray from a Pressurized Metered-Dose Inhaler", *Atomization and Sprays*, Vol. 7, 1997 pp.419-436.
- [5] Bauckhage, K., "The phase-Doppler-difference-method, a new technique for simultaneous size and velocity measurements", *Part. Part. Syst. Charact.* 1988, 5:16-22.
- [6] C.A. Dunbar, "Atomization Mechanisms of the Pressurized Metered Dose Inhaler", *Part. Science and Tech*, 1997, 15:195-216
- [7] "Series 100 Scientific Helium Neon Lasers Instruction Manual", Spectra-Physics, Eugene, OR, U.S.A, 1986.
- [8] J.C. Maxwell, "Collected Scientific Papers", Cambridge 625, 1890.
- [9] N.A. Fuchs, "Evaporation and Droplet Growth in Gaseous Media", Pergamon Press, London, 1959
- [10] F.P. Incropera & D.P. De Witt, "Introduction to Heat Transfer", Wiley, 1990
- [11] Bird. et. al. , "Transport Phenomena", Wiley, 1960.

APPENDIX : Computer Code Used to Implement Simplified Evaporation Model

Code is written in Matlab.

```
% Classical Droplet Evaporation Model
%
%
% Reading in The data file
read1=wkload('rcln01v1',1,0,[2 1 110 3]);
size1=read1([1:109],1);
count1=read1([1:109],2);
velocity1=read1([1:109],3);

read2=wkload('rcln01v2',1,0,[2 1 110 3]);
size2=read2([1:109],1);
count2=read2([1:109],2);
velocity2=read2([1:109],3);

read3=wkload('rcln01v3',1,0,[2 1 110 3]);
size3=read3([1:109],1);
count3=read3([1:109],2);
velocity3=read3([1:109],3);

% Initializing the variables
xdist=[0.004 0.024 0.044];

cinf=0.0;
D=7.01*10^(-6);
L=1.6533*10^5;
kair=0.026;
rhodrop=1310;

Tinf=(273.15+25);
tempold=230;
tempold1=203.15;           %First guess temperature
temp=200;

x=0.0;
csc=0.0;
t=0.0;
sizeplot=0.0;
dist=0.0;

sizelt=size1;

% Loop to calculate size change for each bin size
% Need an outer loop to loop over time, and then an inner loop to
% loop over the bins. This is so that we can obtain size distribution
at each
% time step, or each distance in x. So basically we have to translate
the
% time steps to x distance.
%for x=0.004 0.05

j=1;
k=1;
```

```

l=1;
% This loop removes the sizes with zero velocities
for i = 1:109
    if velocity1(i) ~= 0
        v1(j)=velocity1(i);
        j=j+1;
    end
    if velocity2(i) ~= 0
        v2(k)=velocity2(i);
        k=k+1;
    end
    if velocity3(i) ~= 0
        v3(j)=velocity3(i);
        l=l+1;
    end
end

vlave=mean(v1);
v2ave=mean(v2);
v3ave=mean(v3);

v=[vlave v2ave v3ave];
polyx=polyfit(xdist,v,3);

for k = 1:50;
    if k == 1;
        x1(k)=0.004;
        vel(k)=polyval(polyx,x1(k));
        time(k)=0.0;
    else
        x1(k)=(k-1)/49*0.046+0.004;           %.046 is an arbitrary distance
        vel(k)=polyval(polyx,x1(k));
        vtemp=(vel(k)+vel(k-1))/2;           %Use the average velocity
        if vtemp == 0
            tim=0;
        else
            tim=(0.046/49)/vtemp;           %find the time needed to go
        end
        time(k)=time(k-1)+tim;
    end
end

end

polytx=polyfit(time,x1,3);

cumumass1(1)=(size1(1)*10^(-6))^3*pi/6*1310*count1(1);
cumumass2(1)=(size2(1)*10^(-6))^3*pi/6*1310*count2(1);
cumumass3(1)=(size3(1)*10^(-6))^3*pi/6*1310*count3(1);

% Temperature Iteration
%
while abs(temp-tempold)>0.001
    fold=-L*D/kair*(surfconc(tempold))+Tinf-tempold;
    fold1=-L*D/kair*(surfconc(tempold1))+Tinf-tempold1;
    tempnew=tempold-fold*(tempold1-tempold)/(fold1-fold);
    temp=tempold
    tempold1=tempold;
    tempold=tempnew;
end

```

```

end

cs=surfconc(temp)

% Main loop
%
for i=1:109

    mass1(i)=(size1(i)*10^(-6))^3*pi/6*1310*count1(i);
    mass2(i)=(size2(i)*10^(-6))^3*pi/6*1310*count2(i);
    mass3(i)=(size3(i)*10^(-6))^3*pi/6*1310*count3(i);

    if i ~= 1
        cumumass1(i)=cumumass1(i-1)+mass1(i);
        cumumass2(i)=cumumass2(i-1)+mass2(i);
        cumumass3(i)=cumumass3(i-1)+mass3(i);
    end

%   if count1(i)==0
%       sizeplot(i,2)=0;
%       sizeplot(i,3)=0;
%       sizeplot(i,4)=0;
%       dist(i,2)=0;
%       dist(i,3)=0;
%       dist(i,4)=0;
%   else

d=size1(i)*10^(-6);
j=0;
sizeplot(i,1)=size1(i)*10^(-6);
dist(1)=xdist(1);

    %tempR=(temp-273.15)/5*9+32+459.67;

    %Converting to R=F+459.67
    %P=10^(39.88381727-3436.632228/tempR-
12.47152228*log10(tempR)+4.73044244*10^(-3)*tempR);
    %Pfinal=P*6.89474483; %convert from psi
to kpa
    %cs=Pfinal/0.06876/temp;

fp=0;
sp=0;
    kp=0;
    lt=0;
if d == 0;
    sizeplot(i,2)=0;
    sizeplot(i,3)=0;
    sizeplot(i,4)=0;
    dist(i,2)=0;
    dist(i,3)=0;
    dist(i,4)=0;
else
    for j=1:2000
        dt=1/100000;

```

```

distance=polyval(polytx,j*dt);

if d > 0
    dddt=4*D*(cs-cinf)/(rhodrop*d);
    d=d-dddt*dt;
end

    if d ~= 0
    if d < 0.1*10^(-6)
        d=0;
        enddist(i)=distance;
        lifetime(i)=j*dt;
    end
end

if (distance - .024) >= 0
    if fp ~= 1
        sizeplot(i,2)=d;
        dist(i,2)=distance;
        fp=1;
    end
end
if (distance - 0.044) >= 0
    if sp ~= 1
        sizeplot(i,3)=d;
        dist(i,3)=distance;
        sp=1;
    end
end
if (distance - 0.025) >= 0
    if kp ~= 1
        sizeplot(i,4)=d;
        dist(i,4)=distance;
        kp=1;
    end
end
end
end
end
end

% Plotting routine

plotcount1=count1/sum(count1);
plotcount2=plotcount1;
plotcount3=plotcount1;
plotcount4=plotcount1;

sizecumu1=count1/sum(count1);
sizecumu2=count2/sum(count2);
sizecumu3=count3/sum(count3);

cumuth1(1)=count1(1);
cumuth2(1)=count1(1);
cumuth3(1)=count1(1);
cumuth4(1)=count1(1);

cumucount1=count1;
cumucount2=count1;
cumucount3=count1;
cumucount4=count1;

```



```

        cumuex1(1)=sizecumul(1);
        cumuex2(1)=sizecumu2(1);
        cumuex3(1)=sizecumu3(1);

for i=1:109
    if sizeplot(i,2) == 0
        plotcount2(i) = 0;
        cumucount2(i) = 0;
    end
    if sizeplot(i,3) == 0
        plotcount3(i) = 0;
        cumucount3(i) = 0;
    end
    if sizeplot(i,4) == 0
        plotcount4(i) = 0;
        cumucount4(i) = 0;
    end
    if i >= 2
        cumuth1(i)=cumucount1(i)+cumuth1(i-1);
        cumuth2(i)=cumucount2(i)+cumuth2(i-1);
        cumuth3(i)=cumucount3(i)+cumuth3(i-1);
        cumuth4(i)=cumucount4(i)+cumuth4(i-1);

        cumuex1(i)=sizecumul(i)+cumuex1(i-1);
        cumuex2(i)=sizecumu2(i)+cumuex2(i-1);
        cumuex3(i)=sizecumu3(i)+cumuex3(i-1);
    end
end

figure(1)
plot(sizeplot(:,2)*10^6,plotcount2,'+',size2,count2/sum(count2),'^')
legend('Theoretical','Experimental')
xlabel('Aerodynamic Diameter (micrometers)')
ylabel('Particle Number Fraction')
title('Particle Mass Distribution at 0.024 meters from nozzle')

figure(2)
plot(sizeplot(:,3)*10^6,plotcount3,'+',size3,count3/sum(count3),'^')
legend('Theoretical','Experimental')
xlabel('Aerodynamic Diameter (micrometers)')
ylabel('Particle Number Fraction')
title('Particle Mass Distribution at 0.044 meters from nozzle')

figure(3)
plot(sizeplot(:,4)*10^6,plotcount4,'+',size2,count2/sum(count2),'^')
legend('Theoretical','Experimental')
xlabel('Aerodynamic Diameter (micrometers)')
ylabel('Particle Number Fraction')
title('Particle Mass Distribution at 0.025 meters from nozzle')

figure(4)
plot(lifetime,size1)
ylabel('Aerodynamic Diameter (micrometers)')
xlabel('Droplet lifetime (s)')
title('Droplet lifetimes vs Droplet size')

figure(5)

```

```

plot(size1,count1/sum(count1),'^')
legend('Experimental and Theoretical')
xlabel('Aerodynamic Diameter (micrometers)')
ylabel('Particle Number Fraction')
title('Particle Mass Distribution at 0.004 meters from nozzle')

%these are the cumulative size distributions

figure(6)
plot(sizeplot(:,2)*10^6,cumuth2/cumuth2(109),'+',size2,cumuex2,'^')
legend('Theoretical','Experimental')
xlabel('Aerodynamic Diameter (micrometers)')
ylabel('Cumulative Particle Number Fraction')
title('Cumulative Particle Mass Distribution at 0.024 meters from
nozzle')

figure(7)
plot(sizeplot(:,3)*10^6,cumuth3/cumuth3(109),'+',size3,cumuex3,'^')
legend('Theoretical','Experimental')
xlabel('Aerodynamic Diameter (micrometers)')
ylabel('Cumulative Particle Number Fraction')
title('Cumulative Particle Mass Distribution at 0.044 meters from
nozzle')

figure(8)
plot(sizeplot(:,4)*10^6,cumuth4/cumuth4(109),'+',size2,cumuex2,'^')
legend('Theoretical','Experimental')
xlabel('Aerodynamic Diameter (micrometers)')
ylabel('Cumulative Particle Number Fraction')
title('Cumulative Particle Mass Distribution at 0.025 meters from
nozzle')

figure(9)
plot(sizeplot(:,1)*10^6,cumuth1/cumuth1(109),'+',size1,cumuex1,'^')
legend('Theoretical','Experimental')
xlabel('Aerodynamic Diameter (micrometers)')
ylabel('Cumulative Particle Number Fraction')
title('Cumulative Particle Mass Distribution at 0.004 meters from
nozzle')

```